Modelling of tsunami-induced bore and structure interaction

DOI:
10.1680/jencm.15.00020

Document Version
Accepted author manuscript

Modelling of tsunami-induced bore and structure interaction

Authors

Gede Pringgana MEng, A.M.ASCE
PhD Student, School of Mechanical, Aerospace and Civil Engineering,
University of Manchester, Manchester, UK.

Lee S. Cunningham MEng, PhD, CEng, MICE, MIStructE
Lecturer, School of Mechanical Aerospace and Civil Engineering,
University of Manchester, Manchester, UK

Benedict D. Rogers MEng (Oxon), DPhil
Reader, School of Mechanical, Aerospace and Civil Engineering,
University of Manchester, Manchester, UK

ABSTRACT

A series of 3-D smoothed particle hydrodynamics (SPH) and finite element (FE) models with a domain in the form of a water tank were undertaken to simulate tsunami-induced bore impact on a discrete onshore structure on a dry bed. The fluid motion was simulated using the SPH-based software DualSPHysics. The tsunami-like waves were represented by solitary waves with different characteristics generated by the numerical paddle wavemaker. Numerical probes were uniformly distributed on the structure's vertical surface providing detailed measures of the pressure distribution across the structure. The peak impact locations on the structure's surface were specifically determined and the associated peak pressures then compared with the prediction of existing commonly used design equations. Using the pressure-time histories from the SPH model, FE analysis was conducted with ABAQUS to model the dynamic response of a representative timber structure. The results show that the equations used to estimate the associated pressure for design purposes can be highly non-conservative. By gaining a detailed insight into the impact pressures and structure response, engineers have the potential means to optimise the design of structures under tsunami impact loads and improve survivability.

Keywords: *coastal engineering, hydraulics & hydrodynamics, timber structures, SPH*

1. Introduction

In many parts of the world, structures in low lying coastal areas are at risk of tsunami inundation and can suffer significant damage if they are not adequately designed for the associated hydrodynamic loads. Onshore tsunami waves propagate from the deep ocean towards the shoreline and break when the incident wave height is approximately similar with the water depth. A broken tsunami wave moves inland in the form of a turbulent hydraulic bore (Palermo *et al*., 2009) as captured on video footage of the 26 December 2004 Indian Ocean Tsunami (Nouri *et al*., 2010). In the context of this work, a bore is defined as a steep,

rapidly moving broken wave with an onshore mass flux that can be very destructive (IOC, 2013).

In the major tsunami disasters in 2004 and 2011 the tsunami bore inundation greatly affected shore-based structures including many critical pieces of infrastructure such as railways, nuclear facilities, etc. By far the majority of structures damaged or destroyed in these events were residential buildings. After the 2011 East Japan tsunami, Suppasri *et al*. (2013) stated that 115,163 houses were heavily damaged, 162,015 houses were moderately damaged and 559,321 houses were partially damaged. Many of those houses were constructed from timber. Such timber structures might survive the earthquake that generated the tsunami due to their relatively high strength-to-mass ratio and flexibility but could not resist the hydrodynamic forces resulting from the bore impact.

An improved understanding of residential building response to tsunami loads could help reduce casualties, increase survive-ability of such structures and speed up recovery time post-tsunami. Becker *et al*. (2011) show that a key factor of building response to the external actions is the interaction between the structural components of the building and the wave. The pressure of the tsunami bore can be likened to the pressures attributable to winds which are treated as uniform lateral pressures acting along the entire height of the building. However, in determining tsunami loads, the varying depth of the water, associated velocity and duration of impact are added variables that affect the resulting force and structure response.

Existing design codes and guides around the world present various approaches to quantification of tsunami loads on buildings. The City and County of Honolulu Building Code (CCH, 2000) recommends formulation as shown by Equation (1), adopted from Dames and Moore (1980), to predict hydraulic bore-like wave impact on vertical walls. The Structural Design Method of Buildings for Tsunami Resistance (SMBTR) in Japan developed by Okada *et al*. (2005) also assumed surge force as given by Equation (1). The surge force (F_s) given in Equation (1) results from the summation of hydrostatic and hydrodynamic force components as given by the following expression:

$$F_s = \frac{1}{2}\rho g h^2 b + \frac{1}{2} C_d \rho u^2 h b \tag{1}$$

where F_s is the surge force per unit width of wall, ρ is the density of water, g is the gravitational acceleration, h is the surge height usually assumed equal to the inundation depth or flood level, b is the breadth of impacted structure, C_d is the drag coefficient which is recommended by FEMA 55 (2003) and CCH (2000) as being equal to 2.0 for the case of square or rectangular piles and u is the tsunami flow velocity. The general form of the tsunami-induced flow velocity is $u = C\sqrt{gh}$, where C is a constant coefficient which is assumed by FEMA 55 (2003) and Camfield (1980) as having a value of 2. The substitution of $u = 2\sqrt{gh}$ into Equation (1) results in the surge force (Fs) as follows:

$$F_s = \frac{1}{2}\rho g h^2 b + 4\,\rho g h^2 b = 4.5 \rho g h^2 b \tag{2}$$

Fujima *et al*. (2009) also proposed two equations for a dry flat shoreline configuration based on the maximum water inundation level and the distance of the structure from the

shoreline. The equation expresses the distance of structure from shoreline (D_F) in terms of (h_{im}/D_F), where h_{im} is the maximum inundation depth. For the numerical model presented here the condition where $h_{im}/D_F > 0.05$ is satisfied, the structure is categorized as close to the shoreline, thus the equation that is applicable for an average estimation of force is:

$$F = 1.8\rho g h_{im} B \tag{3}$$

in which B is the breadth of structure. As an appropriate safety factor, Fujima *et al*. (2009) suggests the coefficient of 1.8 in Equation (3) be increased to 3.3. These equations have resulted from small-scale physical experiments for bores propagating over a dry bed.

Robertson *et al*. (2011) categorized the main research on wave impact loads on structures into the following three areas: (i) work related with storm wave impact on offshore platforms which is presently the most commonly studied; (ii) combining experimental and numerical research in order to develop design formulae for associated loads on structures; (iii) research on the forces and associated structural response resulting from tsunami bores impacting on land-based structures. This last area, is least studied. Consequently, there is a need for better understanding of tsunami bore impact on onshore coastal structures due to the relatively limited available research. Following the Indian Ocean tsunami in 2004 and the Tohoku tsunami in 2011, extensive study has been conducted in order to improve the understanding tsunami impact loads and improve design guidelines. However, research has mainly focused on experimental investigation and has been mostly confined to small scale models, while numerical models have been limited due to the high computational demand (Como and Mahmoud, 2013). The research presented herein is intended to address the aforementioned issues by providing more detailed information on tsunami-induced bore and structure interactions via numerical models. The numerical study is conducted using two software packages: (i) the fluid is simulated using the smoothed particle hydrodynamics (SPH) software DualSPHysics; DualSPHysics is a free open-source SPH code released online (see http://www.dual.sphysics.org), (ii) the structural response is simulated using the commercial software ABAQUS. The ultimate goal of the research is to enhance present understanding of tsunami wave-structure interaction with a view to improving current design provisions.

Smoothed particle hydrodynamics is a meshless Lagrangian technique which is ideal for simulating highly nonlinear free-surface phenomena such as tsunami waves. By solving the 3-D Navier-Stokes equations, the SPH numerical modelling technique offers the potential for improved definition of wave characteristics and associated pressures on impacted structures. The capabilities of SPH to model wave-structure interaction for coastal engineering problems were presented by Dalrymple *et al*. (2009), Barreiro *et al*. (2013) and Altomare *et al*. (2015). Previous studies by the authors have demonstrated the applicability of SPH in quantifying tsunami wave characteristics within acceptable levels of accuracy when impacting vertical onshore structures (Cunningham *et al*., 2014). In addition to the laboratory experiments on tsunami wave impact on structures near shore, St-Germain *et al*. (2014) also conducted the numerical modelling using SPH on the basis of analogies between tsunami bores and dam break waves. Furthermore, the SPH technique has also been used to model other violent wave behaviour such as storm wave impact on vertical walls near shore,

(Altomare *et al*., 2015). More details about DualSPHysics program can be found in Crespo *et al*. (2015), Crespo *et al*. (2011), Crespo *et al*. (2013), Gomez-Gesteira *et al*. (2012a), Gomez-Gesteira *et al*. (2012b). Although Canelas *et al*. (2013) have coupled SPH to the discrete element method (DEM) for fluid-structure interaction none of the aforementioned studies have investigated the response of a deformable structure due to the hydrodynamics of a tsunami-like wave. This paper addresses that gap building on the work of (Cunningham *et al*., 2014).

This paper is structured as follows; firstly an overview of the two stages of numerical modelling is given. This is followed by the detailed description of the SPH modelling including model geometry and associated convergence study. Subsequent to this the results from the SPH models including the pressure-time histories that will be applied in the finite element model will be described. Finally, the response of the impacted structures via finite element analysis will be presented and discussed.

2. Methodology

The numerical modelling conducted herein consists of two stages, the first being the simulation of tsunami-like waves followed by the modelling of the response of the wave-impacted structure. The numerical simulations of the tsunami-like wave were conducted using DualSPHysics version 3.0 and were intended to predict tsunami-like bore pressure distributions on the surface of impacted structures. The output obtained from SPH numerical modelling in the form of wave pressure distribution histories are then used as an input in the second stage numerical modelling using the commercially available finite element software ABAQUS/CAE 6.10 to define the structural response of an idealized residential structure. DualSPHysics can perform SPH computational modelling on both central processing units (CPUs) and Graphics Processing Units (GPUs). Hardware acceleration provided by a GPU was performed to take advantage of speed ups of up to two orders of magnitude. In addition to previous studies undertaken by the authors, further validation of the SPH model was conducted by re-modelling the dambreak simulation by Kleefsman *et al*. (2005).

For simulation purposes, throughout this work the tsunami wave is idealised as a solitary wave. This is an idealisation taking advantage of the well-defined and reproducible characteristics of a solitary wave. For discussion on the merits of this approach, the reader is referred to McCabe *et al*. (2014). The variation of solitary wave height, H, was non-dimensionalised using the offshore water depth h_0. Three different cases with different solitary wave heights were performed, H/h_0 = 0.1, 0.3 and 0.5. Other parameters in the modelling were kept constant. The H/h_0 values were expected to give associated bores with specific heights and velocities that are two main factors in the determination of bore impact pressure on onshore structures. The numerical pressures output from each numerical case will be compared with the pressures determined from existing empirical equations that are based on physical experiments for bores propagating over a dry bed.

The tsunami-like wave simulation presented herein uses a small-scale domain. To implement the numerical modelling results in a real condition, normal similarity Froude scaling laws are applied. For practical purposes, the size of idealized structure in the numerical SPH model (1m x 1m x 1m) was scaled up by a factor of 3, where this value was chosen to resemble the feasible size of simple single storey residential shelter made of timber. In line with Froude scaling laws, the SPH pressure output was also scaled up by a factor of 3. The structure's dimensions and the pressure loads after being scaled are then used in the finite element (FE) model. These types of structure were chosen as the focus of the FE modelling because they are fairly typical of the coastal buildings widely damaged by the tsunamis of 2004 and 2011 (Como and Mahmoud, 2013; Suppasri *et al*., 2013). The dimensions and material properties of the representative timber structure's members in the FE model follow the provisions set out in the International Residential Code (ICC, 2009). More details on SPH and FE modelling are explained in the following sections.

3. Description of the SPH Models

The SPH method is based on integral interpolants. Following Barreiro *et al*. (2013), the fundamental principle is to approximate any function $A(\boldsymbol{r})$ by:

$$\langle A(\boldsymbol{r})\rangle = \int_{\Omega} A(\boldsymbol{r})W(\boldsymbol{r}-\boldsymbol{r}',h)d\boldsymbol{r}' \tag{4}$$

where $\boldsymbol{r}$ is position, W is the weighting function or *kernel*, h is the or smoothing length which controls the radius of influence of domain of Ω and $\langle ...\rangle$ denotes an approximation. Equation (4), in discrete notation, leads to an approximation of the function at a particle of interest (interpolant point) a:

$$A_a = \sum_b A_b \frac{m_b}{\rho_b} W_{ab} \tag{5}$$

where the subscript refers to each particle, m is the mass, and ρ is density and the summation is performed over all the particles b within the region of compact support of the kernel function as illustrated by Figure 1.

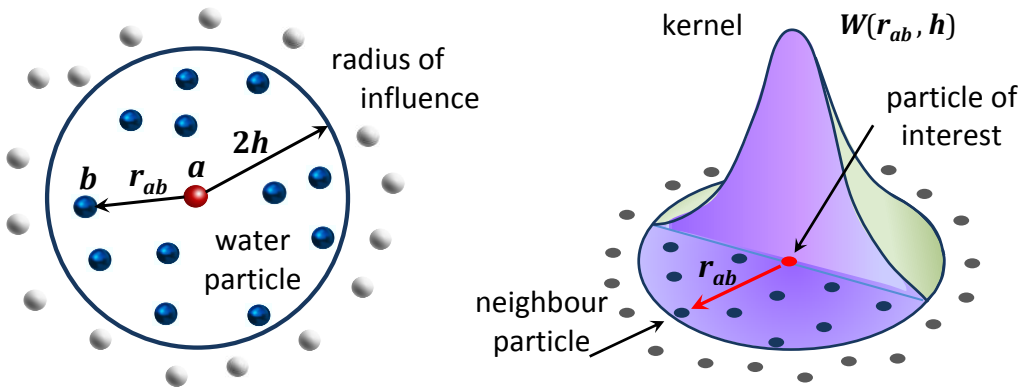

Figure 1 Schematic of the SPH smoothing kernel

The SPH model relies on the selection of the weighting functions that must satisfy the conditions such as positivity, compact support and normalization (Monaghan, 1992). When evaluated for the interaction between two particles a and b the weighting function, W_{ab}, depends on the smoothing length, h, and is normally expressed in terms of the non-dimensional distance between particles given by $q = r_{ab}/h$ where r_{ab} is the distance between particles a and b ($r_{ab} = |\boldsymbol{r}_a - \boldsymbol{r}_b|$). The parameter h controls the size of the area surrounding particle a where the contribution of any other particles inside the area cannot be neglected. In the SPH simulations presented in this paper, the fifth-order Wendland kernel is used. More information on the kernels and the formulation available in DualSPHysics can found in Crespo *et al*. (2015).

As in many weakly compressible SPH (WCSPH) simulations, the kernel approximation and its gradient are not corrected to ensure reproducibility of the constant and linear functions. Although kernel correction is attractive mathematically, and in some SPH formulations essential (notably the incompressible SPH (ISPH) simulations where conservation is discarded in favour of increased accuracy, Lind *et al*. (2012)), it is not essential for WCSPH simulations since the SPH equations conserve the fundamental quantities of mass and momentum (Violeau and Rogers, 2016). Indeed, enforcing reproducibility can make WCSPH unstable while Altomare *et al*. (2015), Barreiro *et al*. (2013), Farahani *et al*. (2014) and St-Germain *et al*. (2014) have shown that WCSPH with no correction gives satisfactory results for nearshore wave processes.

The SPH formalism is used to discretise the governing equations expressing conservation of mass and momentum.

Conservation of Mass

In WCSPH, the conservation of mass equation, or continuity, is solved in Lagrangian form as:

$$\frac{d\rho}{dt} = -\rho\nabla.\boldsymbol{v} \tag{6}$$

where $\boldsymbol{v}$ is the velocity, t is time and ρ is density. The changes in the fluid particle density are determined by solving the conservation of mass or continuity equation in SPH form:

$$\frac{d\rho_a}{dt} = \sum_b m_b \boldsymbol{v}_{ab} \cdot \nabla_a W_{ab} \tag{7}$$

where $\boldsymbol{v}_{ab} = \boldsymbol{v}_a - \boldsymbol{v}_b$ and $\nabla_a W_{ab}$, denotes the derivative of the smoothing kernel W_{ab} with respect to the coordinates of particle a . The mass of each SPH particle is kept constant.

Conservation of Momentum

In Lagrangian form, the momentum equation in continuous form is:

$$\frac{d\boldsymbol{v}}{dt} = -\frac{1}{\rho}\nabla P + \boldsymbol{g} + \boldsymbol{\Gamma} \tag{8}$$

where P is pressure, $\boldsymbol{g}$ = (0, 0, -9.81) ms^{-2} is the gravitational acceleration and $\boldsymbol{\Gamma}$ is the dissipative terms. There are several ways to solve the dissipative terms; however, the most widely used due to its simplicity is the artificial viscosity proposed by Monaghan (1992) and is used herein.

There are numerous forms of an SPH gradient which are chosen according to the physics or numerical properties. With the classical formulation, the pressure gradient in SPH notation uses a symmetric form of the gradient to conserve momentum:

$$-\frac{1}{\rho}\nabla P = -\sum_b m_b \left(\frac{P_a}{\rho_a^2} + \frac{P_b}{\rho_b^2}\right)\nabla_a W_{ab} \tag{9}$$

where P_b and ρ_b are pressure and density of particle b. The artificial viscosity can be included in Equation (9) by adding the viscosity term $\boldsymbol{\Pi}_{ab}$ inside the bracket. Thus, the momentum conservation equation in SPH will be:

$$\frac{d\boldsymbol{v}_a}{dt} = -\sum_b m_b \left(\frac{P_a}{\rho_a^2} + \frac{P_b}{\rho_b^2} + \boldsymbol{\Pi}_{ab}\right)\nabla_a W_{ab} + \boldsymbol{g} \tag{10}$$

The artificial viscosity depends on the relative position and motion of the computed particles

$$\boldsymbol{\Pi}_{ab} = \begin{cases} \dfrac{-\alpha\overline{c_{ab}}\mu_{ab}}{\rho_{ab}} & \boldsymbol{v}_{ab}\cdot\boldsymbol{r}_{ab} < 0 \\ 0 & \boldsymbol{v}_{ab}\cdot\boldsymbol{r}_{ab} > 0 \end{cases} \tag{11}$$

where $\boldsymbol{v}_{ab} = \boldsymbol{v}_a - \boldsymbol{r}_b$, $\mu_{ab} = h\boldsymbol{v}_{ab}\cdot\boldsymbol{r}_{ab}/(\boldsymbol{r}_{ab}^2 + \eta^2)$, $c_{ab} = 0.5\,(c_a + c_b)$ is the mean value of the speed of sound, $\eta^2 = 0.01\,h^2$, and α is a parameter whose value ranges from 0.01 to 0.5, that should be adjusted according the configuration of the problem.

In the simulations presented herein, a 3-D SPH numerical water tank is used for simulating near-shore and onshore areas. In DualSPHysics, the implemented boundary conditions include the Dynamic Boundary Conditions (DBCs) for solid walls (Crespo *et al*., 2007) and the Periodic Boundary Conditions (PBCs) for lateral open boundaries (Gomez-Gesteira *et al*., 2012). To represent a solid wall, the dynamic SPH boundary was used for the numerical model. The boundary particles (BPs) and the fluid particles (FPs) in the DBCs satisfy the same equations but are not allowed to move (the movement is equal to zero) in any direction except where externally imposed such as a flap or a piston in a wave maker. In the DualSPHysics code, the initial geometry, configuration and case parameters are defined in the Extensible Markup Language (XML) input file and this also includes the size of particles. In the following subsections, first the particle size required to capture the pressure due to the bore impact is identified, and second, this information is then used to model the tsunami bore impacting the structure.

3.1 Choosing the particle size (d_p): convergence study for bore impact.

The choice of water particle size or the initial spacing of particle (d_p) is crucial in SPH modelling. The particle size influences the overall simulation including the behaviour of

waves, the accuracy of pressure prediction and the time of simulation. The particle size was determined using a numerical convergence study by re-modelling the dambreak impact on a box case in Kleefsman *et al*. (2005) as suggested by the SPH European Research Interest Community (SPHERIC) for relevant model validation. The use of the dambreak case for validation purposes is based on the assumption that the bore characteristics of the tsunami are closely represented by a broken dambreak wave front (Chanson, 2006). This case has been used previously for validation to demonstrate convergence (Crespo *et al*., 2011), here the maximum particle size required to capture the impact pressures is identified.

The fluid flow properties in the convergence study were the impact pressure and the water level. Many parameters influence the pressure and the water level but in this case their values were kept constant for all models and only the particle size (d_p) was modified following previous work by the authors, (Cunningham *et al*., 2014). The only execution parameter recently added in this model is the "δ-SPH" where the value was equal to 0.1. The δ-SPH is one of some improvement in DualSPHysics version 3 that was used for all SPH models in this paper. The δ-SPH scheme virtually eliminates unphysical pressure fluctuations and thereby enhances the pressure prediction of an SPH model involving violent waves.

A convergence study is needed to determine the largest particle size and hence shortest runtime that can use in a simulation to capture hydrodynamics. The shortest dimension in the associated dambreak model that was used as a reference was the height of the impact-target structure in the form of a box equal to 0.161 m (see Figure 2a). The height of the box is denoted herein by *L*. The convergence study for the pressure predicted at P_1 is depicted in Figure 2b where three different values of d_p are compared. It can be seen that the d_p value equal to *L*/20 gives the closest prediction to the experiment results. Using d_p values smaller than *L*/20 shows little improvement and is too computationally expensive to be implemented. The GPU specification and run-times are given in Table 1. A list of key constants and execution parameters in the XML input file used in this study are given in Table 2. The prediction of the smaller d_p values is not presented here. Following the results of the convergence study, the diameter of particle (d_p) representing fluids and solid parts in the model domain was set equal to 0.05 m or 1/20 of the still water level (h_0) or the height of structure (*D*) that was in this case set to be 1 m, this led to 639,698 particles. Other SPH simulations that can be considered as convergence studies were the modelling of experimental works by Linton *et al*. (2013) and Zhang (2009) that can be found in previous work by the present authors (Cunningham *et al*., 2014).

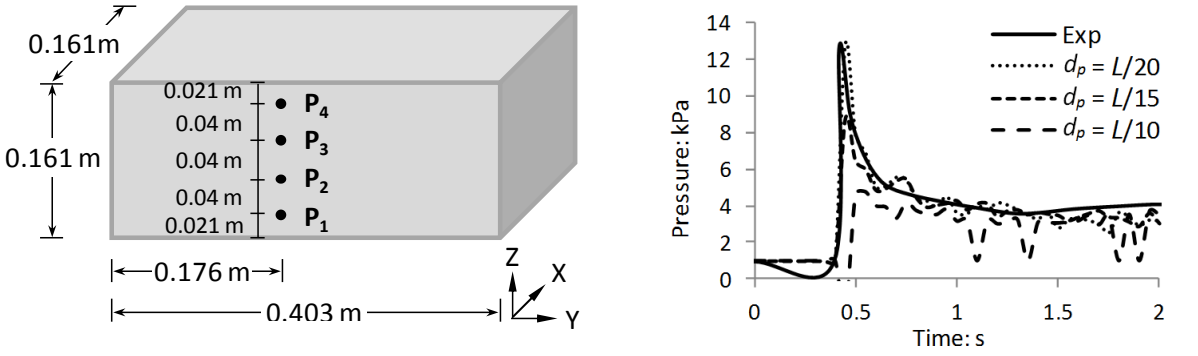

(a) Box dimension and probes position (b) SPH pressure at probe P1

Figure 2 Dambreak case for SPH validation

Table 1 GPU specification used in the modelling and the run-times

GPU Specifications		SPH model details (DualSPHysics v3.0)	
GPU type	Tesla M2050	Particle size	0.05 m (L/d_p = 1/20)
Memory global	2687 Mb	Total particle	639,698
Number of cores	488	Time out	0.025
Clock rate	1.15 GHz	Total run time	36 minutes

Table 2 Key XML parameters for input into DualSPHysics

Constants		Execution parameters	
Particle size d_p (m)	0.05 m	Step algorithm	2 (Symplectic)
Lattice number	bound = 2, fluid =1	Kernel	2 (Wendland)
Cfl number	0.2	Visco treatment	1 (artificial)
Coefficient of sound	10	Viscosity	0.1
Eps value	0.25	Shepard step	30

3.2 Description of geometry of the SPH model

Having established the particle size required to capture the pressure history on the face of an obstacle similar to those being studied, the focus of the article now shifts to simulating the input of a tsunami-type bore on a structure near the shoreline.

The geometry of the SPH numerical domain is shown in Figure 3 where a notation of D is used in the model to represent its characteristic length of 1 m. The size of model components or lengths in the geometry is given as a multiple of D, for example, the size of structure and the depth of still water are D, the distance of the structure to the shoreline and to the rear boundary wall are $2D$, and the width of water tank and the height of paddle

wavemaker are $3D$. This was intended to non-dimensionalise the analysis results. Figure 3 indicates the direction from where the pressure distribution can be viewed and this is the viewpoint (shown by the eye symbol) used for the snapshots shown later.

The dimensions of the numerical water tank here are 15 m long, 3 m wide and 5 m high. The numerical domain consists of a flat offshore region containing water particles, a sloping sea bed and onshore region where the coastal structure is placed. In a 3-D model, the boundary line for the sloping bed (before shoreline) could be the location where water particle penetration occurs. To prevent an occurrence of excessive fluid particles out of the boundary, a double layer of particles is used for the boundary line by setting the "lattice number" equal to two. Excessive out-of-boundary fluid particles could reduce the amount of fluid particles inside the tank and could affect the wave propagation (reduce the water surface elevation), especially when it undergoes a long propagation. For all models in this study, the percentage of the out of boundary fluid particles was limited to less than 1 percent of the total amount of fluid particles involved.

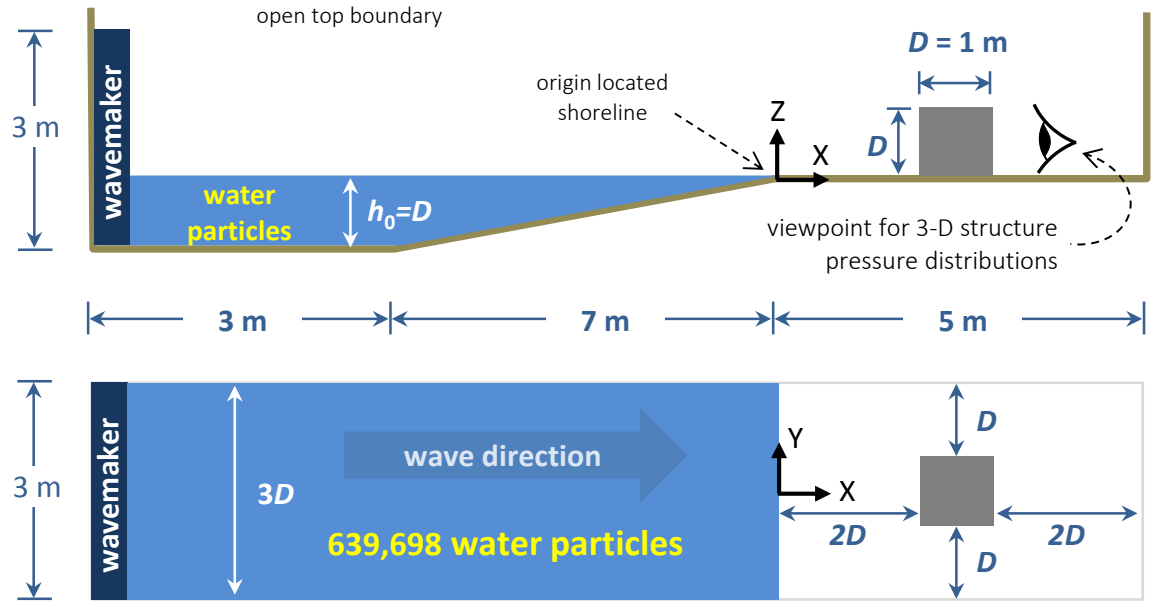

Figure 3 Side and plan view of 3-D model with simple structure (not to scale)

The parameter varied in the simulations is the wave height based on a ratio between targeted wave height and still water level (H/h_0). Three different values of H/h_0 were used: 0.1, 0.3 and 0.5, these provide the respective wave height 10, 30 and 50 cm for h_0 equal to 1 m. Those wave heights resulted in bores when reaching onshore and subsequently impacted the on-shore structure. A rectangular structure was chosen as representative of a coastal structure and hence impact target. The dimensions of the rectangular structure are 1m x 1m x 1m. The incoming wave was expected to hit the vertical sides of cube that was perpendicular to the incoming wave direction. The distance of vertical side of the cube was set $2D$ (2 m) from the shoreline.

The origin for the numerical models lies within the model domain and located at the shoreline. Since DualSPHysics is a single precision code, the position of zero axes can influence the accuracy of measurements of quantities such as pressure. In other words, a model with the zero axis located somewhere inside the domain performs better than when its zero-axis position is situated at the end of or much further from the model domain (Longshaw and Rogers, 2015). Another advantage of the zero axis position inside the domain, at the shoreline in this model for instance, is the ease of modifying parts of the model at both ends of the water tank. For example, when it is necessary to adjust the paddle distances from the shoreline or change the positions of the target structure (together with the measuring probes) at the opposite end of the water tank, it can be done without changing large parts of the *XML* input file.

4. Computing SPH pressures and forces on the structure

The DualSPHysics software provides output in the form of pressure-time history measured by numerical measuring probes. This pressure value can be used to estimate the force. As illustrated in Figure 4, the force (F_i) at a certain point in a 3-D model can be determined by multiplying the pressure (P_i) with the area (A_i) of probe i, see Equation (12). Hence, the total force (F) acting normal to a surface can be estimated by summing the force acting on the total number (n) of areas used to represent the object surface, see Equation (13).

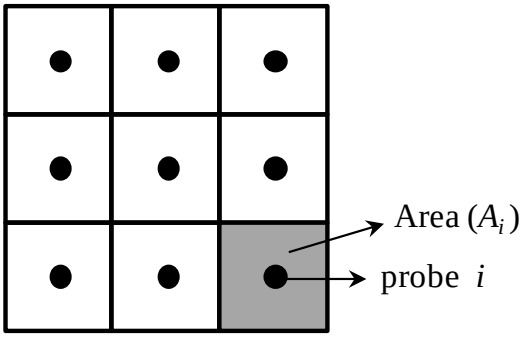

$$F_i = P_i A_i \tag{12}$$

$$F = \sum F_i = \sum_i^n (P_i A_i) \tag{13}$$

Figure 4 Arrangement of probes on the face of the obstacle

Numerical measuring probes were placed at several locations inside the model domain. The pressure probes were evenly distributed on all surfaces of the target structures shown in Section 6. The spacing of pressure probes on the structure's surface facing the incoming waves is 0.1 m or twice the diameter of particles as the interpolation region around each probe (which is approximately twice the smoothing length or particle size in radius) is sufficient to capture the peak pressure. For the vertically-arranged measuring pressure probes, the probes start at a height of 0.05 m from the bed. Probes for measuring wave velocity and wave height were placed along the longitudinal axis of the tank (see Figure 5).

5. SPH Modelling Results and Discussion

5.a. Water surface elevation

Previous validation for the SPH water surface elevation generated by solitary wave was presented by Cunningham *et al*. (2014). Here, we present the results for different wave height to water depth ratios. Figure 5 shows the probe positions for measuring water surface elevation regarding the propagation of the solitary wave for cases with different H/h_0. The water surface elevations were measured at certain probes along the tank. H1 is placed 1 m from shoreline and followed by H2 through H7 at a constant 1 m spacing apart. The properties of the offshore solitary waves and onshore bores can be seen from Figure 6 and Figure 7 and also from Table 3.

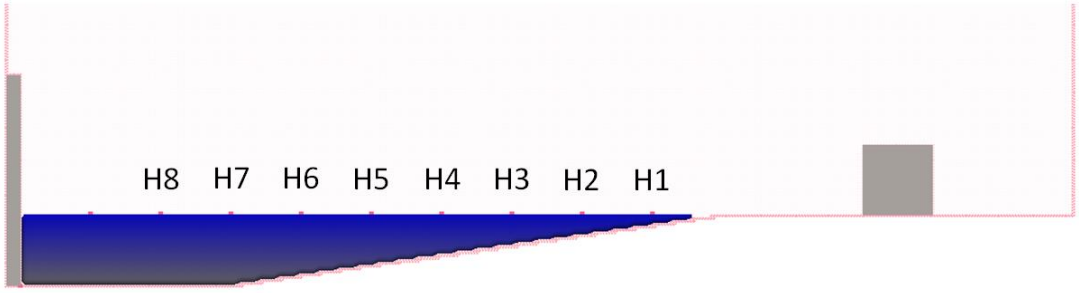

Figure 5 Layout of water surface elevation probes H1-H7

Figure 6 depicts the SPH simulation of the solitary wave propagation offshore for the case with H/h_0 = 0.5. From the four snapshots given in Figure 6a to Figure 6d, the changes in the solitary wave profile/shape can be observed. Near the shoreline at probe H1, the solitary wave started to break and its elevation decreased as illustrated in more detail in Figure 7.

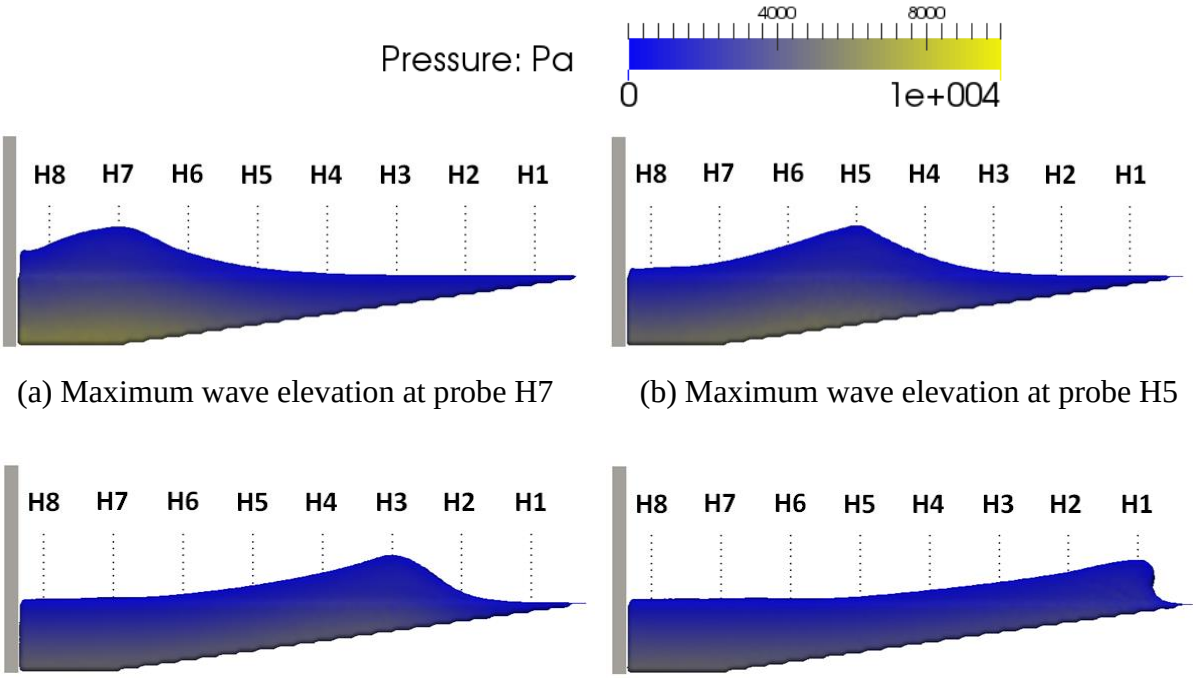

(a) Maximum wave elevation at probe H7

(b) Maximum wave elevation at probe H5

(c) Maximum wave elevation at probe H3

(d) Maximum wave elevation at probe H1

Figure 6 SPH simulation of solitary wave height and pressure during propagation from probe H7 through probes H1 for case with H/h_0 = 0.5

Figure 7 shows the comparison of solitary wave elevations based on different H/h_0 during propagation towards the shoreline. The surface elevations were measured at four different probes H7, H5, H3 and H1. The wave elevations were measured from the surface of water at rest. From H7 until H1, it can be seen that generally the solitary wave elevation slowly decreases. The maximum elevations of the solitary wave for the case with H/h_0 = 0.5 is almost 100% higher than the case with H/h_0 = 0.3, and almost three times higher than the case with H/h_0 = 0.1. The differences in wave elevation correspond to the differences of the associated bore impact forces on the structure. It can also be seen that there are time differences regarding the maximum wave elevations when they reach the probes.

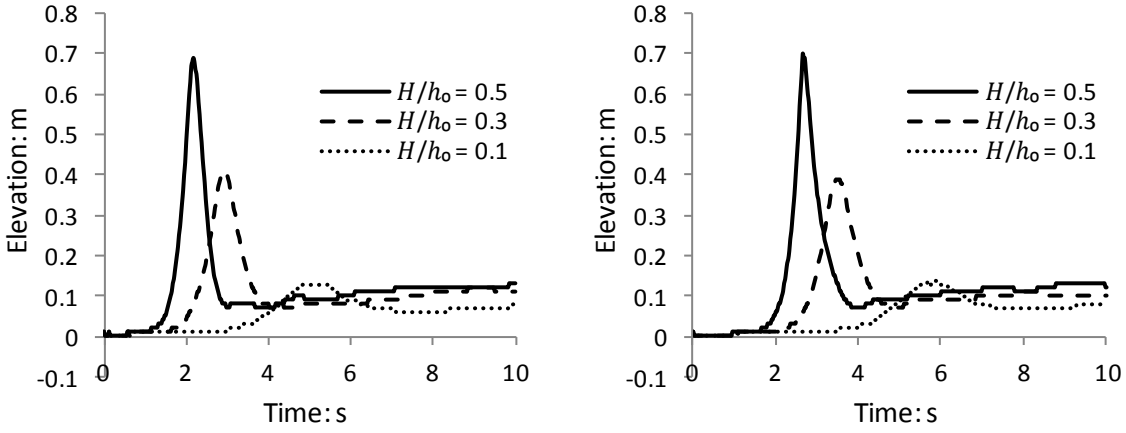

(a) Probe H7 (b) Probe H5

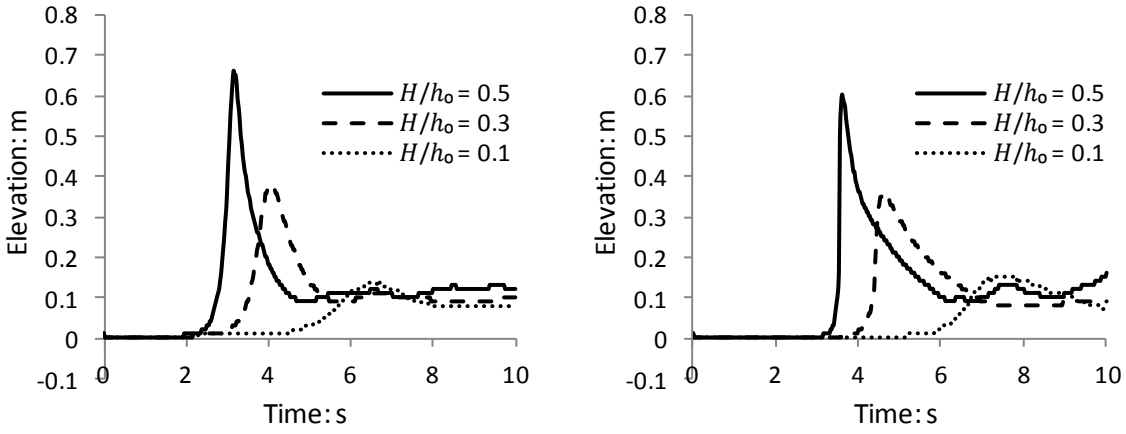

(c) Probe H3 (d) Probe H1

Figure 7 Comparison of solitary wave elevations for different H/h_0 measured at probe H7, H5, H3 and H1.

5.b. Bore Height and Velocity

The onshore bore heights and velocities were measured by probes placed in front of the structure. The values of these properties are important in determining the exerted pressure on the surface of structure. The snapshots of the bores including velocities can be seen in Figure 8 and the variation of bore heights are depicted in Figure 9, for simulation cases with H/h_0 = 0.3 and 0.5.

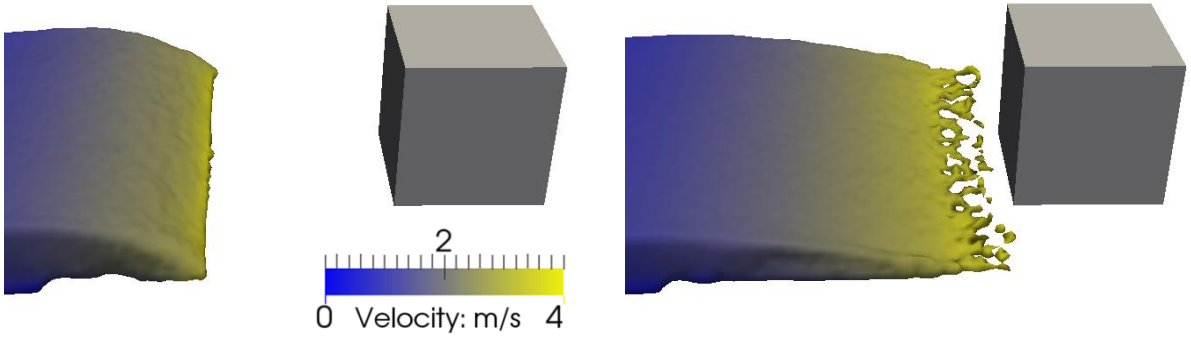

(a) (b)

Figure 8 SPH simulation of bore velocity for the case with H/h_0 = 0.5: (a) near the shoreline and (b) onshore.

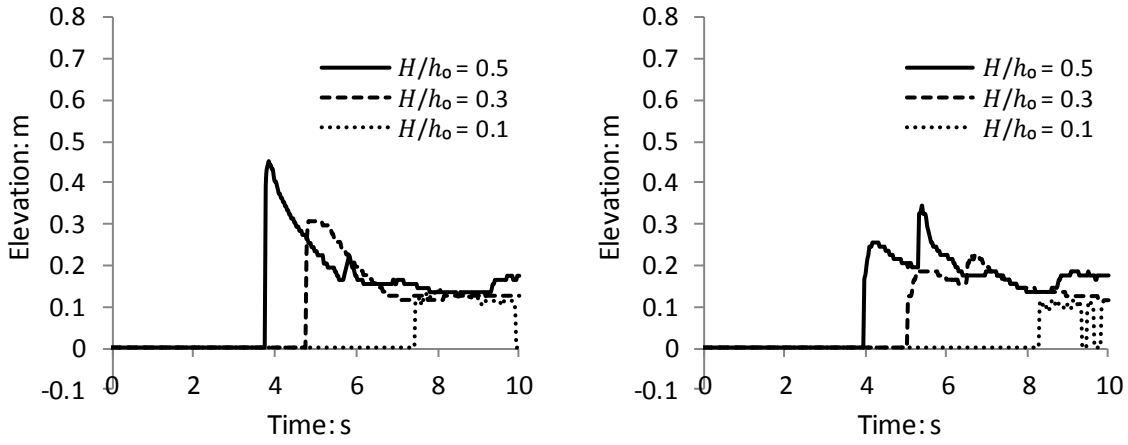

(a) Shoreline (b) Onshore

Figure 9 Bore height measured from still water level at (a) shoreline, (b) onshore.

Table 3 shows the offshore water surface elevation and wave length of solitary waves and the corresponding onshore bore characteristics (height and velocity). It can be observed that offshore, the maximum velocity increases proportionally with the design height of the solitary wave, but inversely proportional to the wave length of the wave. The maximum solitary wave velocities offshore are also proportional to the bore height and velocity onshore.

Table 3 Solitary wave and bore properties

H/h_0	Offshore solitary waves			Onshore bores	
	Maximum elevation	Maximum velocity	Wave length	Maximum height	Maximum velocity
0.5	0.7 m	3.94 m/s	5.0 m	0.32 m	5.65 m/s
0.3	0.4 m	2.13 m/s	6.5 m	0.20 m	4.05 m/s
0.1	0.15 m	0.68 m/s	7.7 m	0.11 m	1.19 m/s

5.c. Wave Pressure

Typical output from the 3-D SPH simulation is shown in Figure 10 and Figure 11 for the case with H/h_0 = 0.5. Figure 10a depicts the snapshot of a propagating solitary wave which is then followed by a bore impact on the structure as shown by Figure 10b. The peak pressure impact occurred at t = 4.150 sec and the peak pressure took place at the lowest level of pressure probes as indicated by the circle in the Figure 10a. In addition, Figure 11b shows the pressure distribution for the maximum bore run-up on the surface of the structure that occurred at t = 4.325 sec and corresponding with Figure 10b. Pressure distributions in Figure 11 were seen from the rear of the structure (see illustration indicating direction of view in Figure 3) by assuming the cube structure is visually transparent.

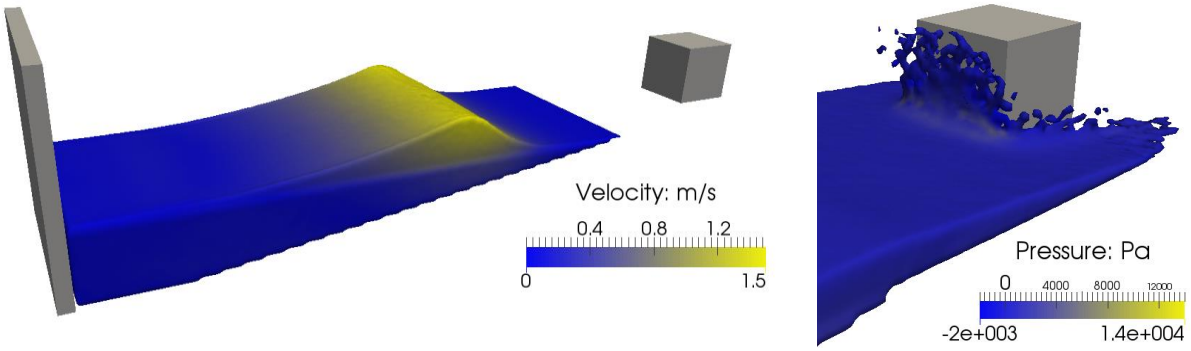

(a) (b)

Figure 10 Oblique view of the 3-D simulation for case $H/h_0 = 0.5$; (a) solitary wave propagation at $t = 3.150$ sec. (related with Figure 6c), (b) bore impacting structure at $t = 4.325$ sec.

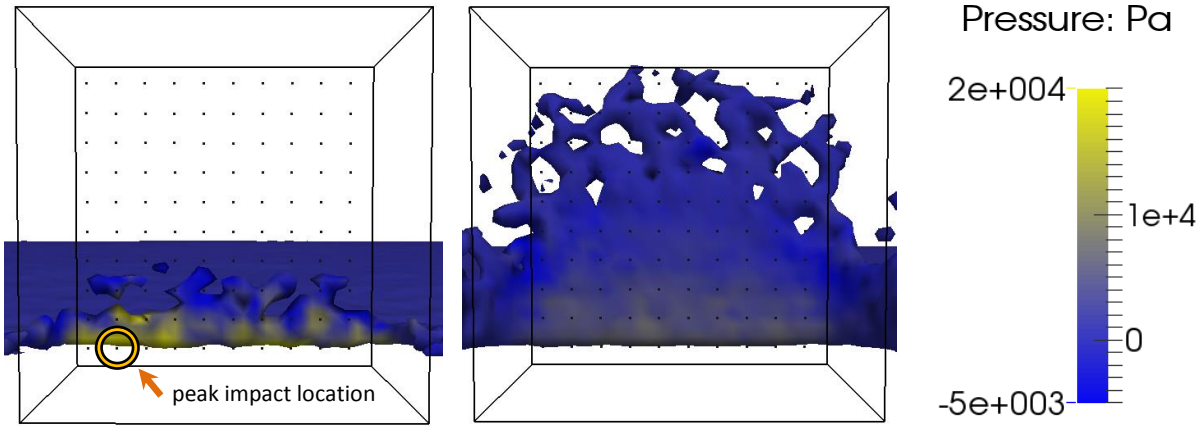

(a) (b)

Figure 11 Pressure distribution on vertical surface at $H/h_0 = 0.5$; (a) first impact at $t = 4.150$ sec, (b) peak impact occurred at the circled probe at $t = 4.325$ sec.

The normalised peak pressures ($P/\rho g h_0$) for the simulation with H/h_0 = 0.1, 0.3 and 0.5 were 0.748, 18.165 and 83.287, respectively. The bore pressures for the case with H/h_0 = 0.1 were comparatively small and resulted in a correspondingly small impact force. Hence, the comparison of the predicted impact pressure between the numerical and the empirical equation were made only for the case with H/h_0 = 0.3 and 0.5. The numerical maximum pressure for the case with wave height equal to H/h_0 = 0.3 and 0.5 were 10,508 N/m^2, and 37,371 N/m^2, respectively. The associated pressures determined by Equation (2) were 1,766 N/m^2 and 4,520 N/m^2 over the bore height for the case with H/h_0 = 0.3 and 0.5, respectively. In addition, the impact pressures predicted by Equation (3) were 3532 N/m^2 and 5651 N/m^2 over the bore height for the case with H/h_0 = 0.3 and 0.5, respectively. However, these results must be viewed within the context that in general the design equations adopt a quasi-static approach to wave pressures, whereas in reality the peak pressure occurs over a very short time period and may be very localised.

6. Finite Element Modelling

The finite element modelling was conducted to study the behaviour of a simple dwelling type structure made of timber under tsunami-like wave bore impact loading. The response of the structures, especially the stress distribution on the main load-bearing components i.e. the vertical studs, will be compared with the behaviour resulting from the quasi-static pressure given by Equation (2).

The dynamic analysis was performed using ABAQUS Explicit (ABAQUS, 2010). In this procedure the equations of motion are integrated in time explicitly using central difference integration rules. The analysis procedure requires a small time increment and since it does not need to solve a global set of equations in each increment, the computational cost per increment is relatively small compared with the implicit method. The explicit method is well suited to modelling short duration/transient loads such as those associated with tsunami wave impacts.

6.1 Model Properties

Figure 12 shows a definition sketch of the timber structure. As previously stated, the structure dimensions for the FE model are 3m x 3m x 3m. The target structure consists of four vertical walls and a flat roof all composed of sandwich timber panels. The sandwich panel is an arrangement of sheath-stud-sheath. The sheath is made of plywood with 13 mm thickness and has the following material properties: density = 750 kg/m^3, Young's modulus = 7.7x10^9 N/m^2 and Poisson's ratio = 0.22. The studs are made of softwood timber (Douglas fir) with a cross sectional size of 38 mm wide x 140 mm deep and installed with spacing centres of 420 mm. The studs' material properties are as follows: density = 530 kg/m^3, Young's modulus = 7.0x10^9 N/m^2 and Poisson's ratio = 0.22. The timber structure was designed to be simply supported at the base i.e. no rotational fixity. The timber structure components were modelled using 8-node linear brick elements (type C3D8R) with reduced-integration and hour-glass control.

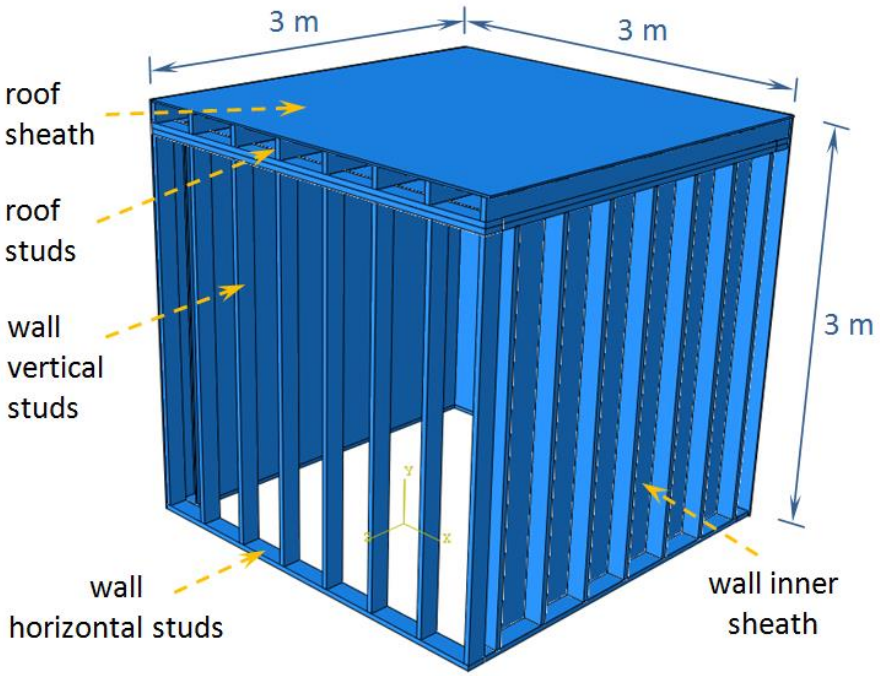

Figure 12 Timber structure general arrangement (wall sheaths removed for clarity as shown).

6.2 Input Loads

The applied pressure-time histories on the FE model structures were obtained from the DualSPHysics output. As mentioned earlier in Section 2, the size of structure in the FE model was scaled up by a factor of three from the structure in the DualSPHysics model. Thus, following dimensional analysis, the magnitude of applied pressures on the surface of the FE models was also scaled up by three from the DualSPHysics output pressures. The pressure-time histories of applied loads can be seen in Figure 13, for both wave simulation cases with H/h_0 = 0.3 and 0.5. The output pressure from the wave simulation with H/h_0 = 0.1 was not included in the FE model analysis because the magnitude was relatively small. The FE structure responses were studied by applying two different pressure time histories (as shown in Figure 13) on the front surface of the structure. One of the key aspects in this method is the application of the same size for pressure probe spacing in the DualSPHysics model with the size of the mesh element in the ABAQUS model. Using the same particle and mesh size enables the output pressure values from the DualSPHysics "MeasureTool" to be applied directly to element in the ABAQUS model. The "MeasureTool" provides pressure values over time in the form of tabular data for each SPH pressure probe. The pressure tabular data for each probe is transferred to the ABAQUS element by using the "load amplitude" and "tabular" options in ABAQUS. The simulations were then run using the dynamic explicit time stepping explained previously.

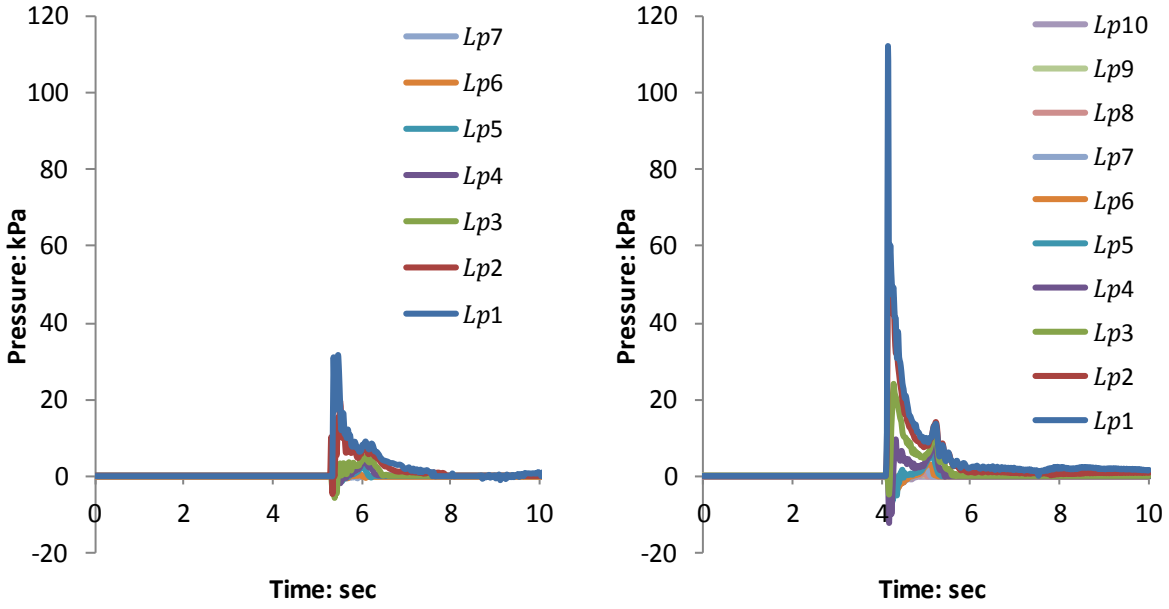

(a) H/h_0 = 0.3 (b) H/h_0 = 0.5

Figure 13 Applied pressure time histories for the finite element models.

The pressures applied on the vertical surface of the structures were divided into 10 layers. This number of layers was identical with the number of probes arranged vertically in the SPH model, denoted by *Lp* in Figure 13. The magnitude of pressure at each layer is the average pressure measured by pressure probes at the associated layer. The reason for applying average pressure history at each layer was based on time efficiency. Also, it was found that the pressure variation measured by SPH probes within the same layer is generally not significant. Figure 13(a) shows the applied loads presented from Layer 1 to Layer 7 (*Lp*1 to *Lp*7). Loads at Layer 8 to Layer 10 (*Lp*8 to *Lp*10) are zero so they were not included in the graph. In Figure 13(b) all 10 layers were loaded. The loaded layers on the surface were related with the height of bore runup on the surface of the wall.

The negative pressure values in Figure 13 reflect the application of the equation of state in DualSPHysics and a rebound or suction effect. DualSPHysics version 3.0 is still a single phase model that cannot yet perform multiphase behaviour including air and water at the same time. The next version of DualSPHysics (version 4.0) is being developed to be capable of performing such multi-phase modelling (Mokos *et al*., 2015). Two peaks are shown in the pressure-time histories in Figure 13. The first peak occurred when the leading edge of the bore impacted the structure and the second peak occurred when the splashing followed with the main flow. These two peak phenomena are typical for impact loads of this type and were also observed in the experiment by Fujima *et al*. (2009). Note in the case of the immediate impact on the structure, no additional force is applied e.g. drag force. The hydrodynamic 'drag' forces indeed occur in real tsunami events (Yeh *et al*., 2014) and affect the structure when surrounded by a 'steady' fluid flow with relatively constant velocity (FEMA, 2011). However in this simulation, the hydrodynamic drag was not so significant

(see Figure 14) because of the application of a single stroke solitary wave where the most dominant effect was the highly transient impulsive pressure immediately following the impact of the leading edge of the arriving water mass.

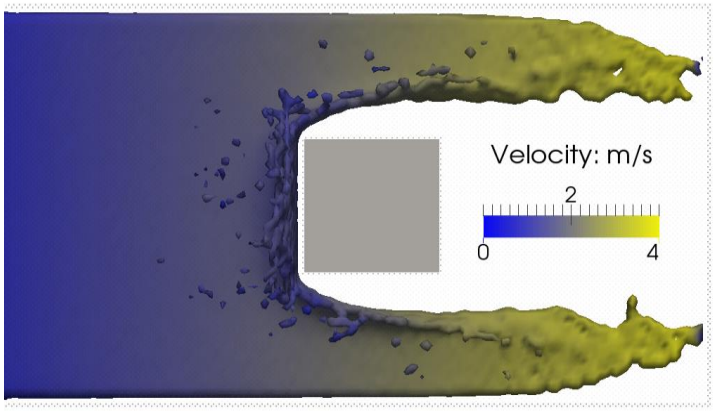

Figure 14 Plan view of SPH simulation showing no significant drag force on the sides of structure.

6.3 Analysis and Results

The finite element analysis was performed using the ABAQUS Dynamic Explicit module with duration of simulation of 2.6 seconds and time increment automatically determined by the program. The duration of simulation was enough to capture the important segment of pressure-time histories given in Figure 13 incorporating the peak impact and subsequent impact. All components of the structure were meshed with the finest mesh on the front surface. The size of the mesh for the front impacted surface was 0.05 m to correspond with the diameter of SPH fluid particles, a coarser mesh with twice the size of elements was used for the other sides of the structure. The response of the structures is shown in terms of the maximum principal stress that occurred on the members. On the front face of the structure, the main load carrying elements are the vertical and horizontal studs and these are shown in Figure 15 by removing the outer plywood cover sheath.

The results of the finite element modelling can be seen in Figure 15 which consists of five figures showing the response of the structure under different loading conditions. Figure 15(a) and Figure 15(b) shows the response of structures loaded by the SPH pressure time-history resulting from a normalised wave height H/h_0 = 0.3 and 0.5, respectively. Figure 15c and Figure 15(d) on the other hand show the response of the structure under a quasi-static pressure determined using the semi-empirical approach given by Equation (2) using the equivalent wave properties. The pressures related with Figure 15(c) and Figure 15(d) were calculated based on a bore height of 0.60 m and 0.96 m, respectively, where those bore heights were taken from the SPH model simulation (see Table 3) and scaled-up by a factor of 3. The application of those bore heights in Equation (2) was intended to accomplish straightforward comparison of the structure's response based on numerical and semi-empirical approaches.

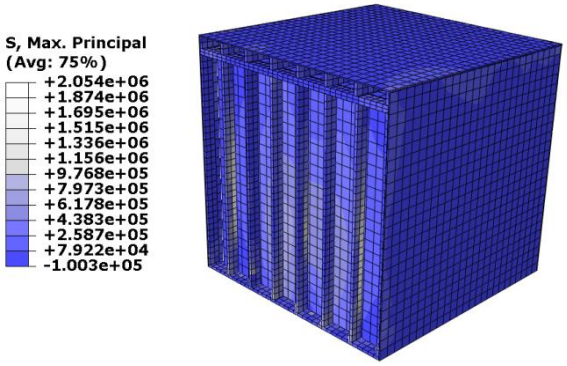

(a) SPH-based pressure (case $H/h_0 = 0.3$)

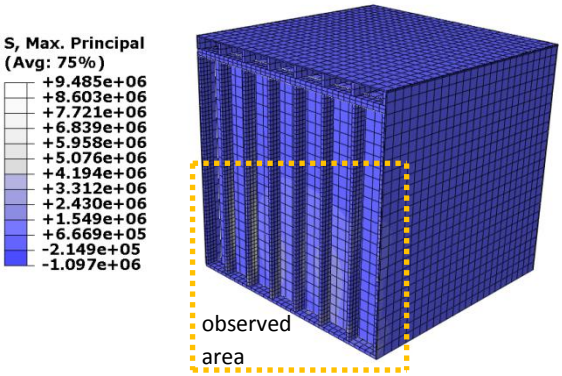

(b) SPH-based pressure (case $H/h_0 = 0.5$)

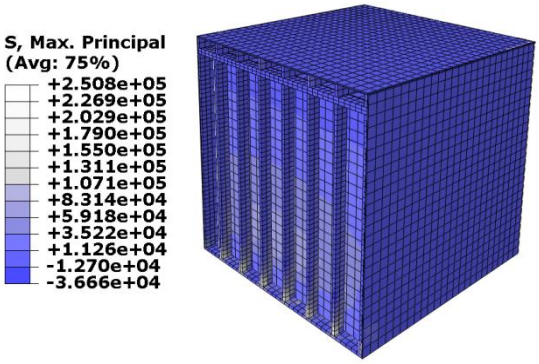

(c) Quasi static-based pressure (case $H/h_0 = 0.3$)

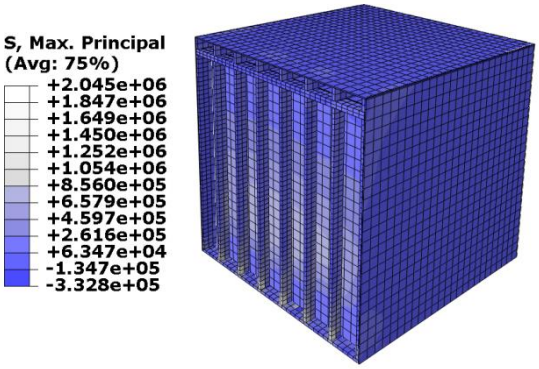

(d) Quasi static-based pressure (case $H/h_0 = 0.5$)

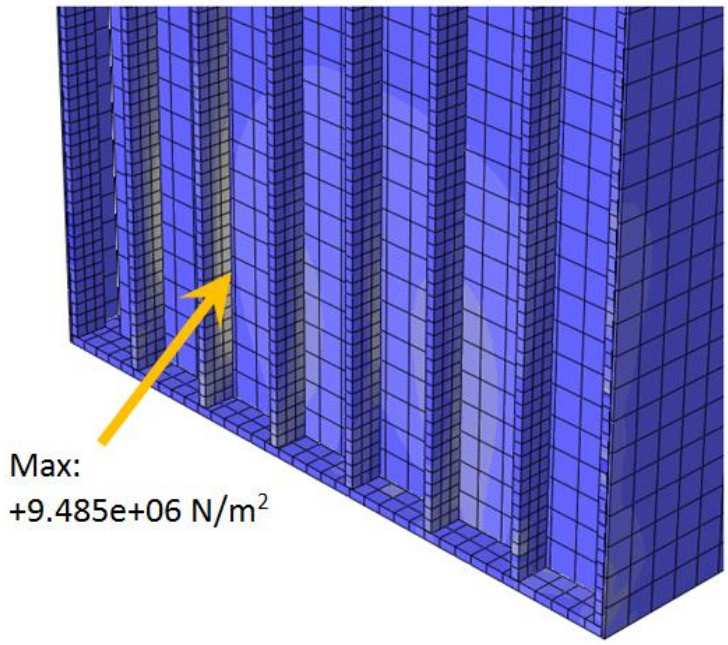

(e) Close up view of area of maximum stress indicated in Figure 15(b).

Figure 15 FE Dynamic response due to SPH pressure-time history (a, b); FE static response due to quasi-static pressure from Equation (2) (c, d); location of maximum stresses (e); (all stresses shown in N/m^2).

Figure 15(a) and Figure 15(b) show that the maximum principal stresses occurred at the tension side, below the mid-span of the vertical studs. The stresses shown in Figure 15(a) and Figure 15(b) are the maximum stresses that occurred at any time in the response to the bore impact and not necessarily simultaneous with the maximum impact pressure. In the case of Figure 15(b), the stresses are approaching the flexural capacity for this type of timber. This general type of flexural failure is in line with experimental results reported by (Lacroix and Doudak, 2014) whereby the vertical studs on timber panels failed due to the out of plane high strain rate induced by blast loading, while in this case the tsunami impact load could also be categorized a high strain rate event as indicated by the pressure time histories in Figure 13. For comparable scale structures, similar failure patterns of timber studs in flexure due to tsunami-like wave impact was reported experimentally by Linton *et al*. (2013). It can also be seen that under higher loads (Figure 15b) the stress concentration tends to develop closer to the lower end of the studs in comparison with Figure 15(a). In this case, a shear-type failure of the stud would be expected. Figure 15(c) and Figure 15(d) show the response of the structure under the static loads resulting from Equation (2). It can be seen that the maximum stresses concentrated at the bottom end of the vertical studs. This response is due to load being applied on the lower part of the structure over the height of the bore. In both Figure 15(c) and Figure 15(d) it should be noted that the predicted quasi-static pressures resulted in timber stresses at least 4 times less than those observed in the dynamic response using the SPH derived pressure-time histories. In real terms, these values represent the difference between the focussed structure remaining intact or not.

7. Conclusions

In this paper, the interactions between a tsunami bore and an idealized timber structure were modelled using the SPH based software DualSPHysics coupled with finite element analysis using ABAQUS. The SPH models show the ability of this approach to provide impact pressure distributions in a great level of detail both spatially and temporally. The results from the SPH models were utilized in the finite element model to predict the response of the structure under transient bore impact loads. The numerical pressure predictions were also compared with pressure predictions from semi-empirical approaches used in design codes. The structure response results highlight the potential for non-conservatisms in the empirical approaches. The techniques outlined in this paper can allow engineers to gain a better insight into tsunami wave-structure interaction and thus lead to resilience optimisation of structures vulnerable to these type of events. Further development is needed for more complex tsunami-like bore and structure interactions including the effect of aeration via multi-phase SPH wave modelling.

8. Acknowledgements

The authors gratefully acknowledge the contribution of the Directorate General of Higher Education of The Republic of Indonesia to the funding of this research. Support from

Warmadewa University of Bali, Indonesia, is also appreciated. Thanks are due to Dr Athanasios Mokos for his assistance with DualSPHysics modelling.

References

ABAQUS. (2010). *ABAQUS analysis user's manual.* Providence, Rhode Island, USA., SIMULIA, Dassault Systèmes.

Altomare, C., Crespo, A. J. C., Domínguez, J. M., Gómez-Gesteira, M., Suzuki, T., & Verwaest, T. (2015). Applicability of Smoothed Particle Hydrodynamics for estimation of sea wave impact on coastal structures. *Coastal Engineering*, *96*, 1–12.

Barreiro, A., Crespo, A. J. C., Domínguez, J. M., & Gómez-Gesteira, M. (2013). Smoothed Particle Hydrodynamics for coastal engineering problems. *Computers & Structures*, *120*, 96–106.

Becker, A. B., Johnstone, W. M., & Lence, B. J. (2011). Wood frame building response to rapid-onset flooding. *Natural Hazards Review*, *12*(2), 85–95.

Camfield, F. (1980). *Tsunami engineering*. *Special Report SR-6*. Coastal Engineering Research Center, U.S. Army Corps of Engineers, Springfield, VA.

Canelas, R., Ferreira, R. M. L., Crespo, A. J. C., & Domínguez, J. M. (2013). A generalized SPH-DEM discretization for the modelling of complex multiphasic free surface flows. In *Proceedings of the 8th International SPHERIC Workshop* (p. 6). Trondheim, Norway.

CCH. (2000). *City and County of Honolulu Building Code (CCH)*. Chapter 16, Article 11. Department of Planning and Permitting of Honolulu Hawaii, Honolulu, HI.

Chanson, H. (2006). Tsunami Surges on Dry Coastal Plains: Application of Dam Break Wave Equations. *Coastal Engineering Journal*, *48*(04), 355–370. http://doi.org/10.1142/S0578563406001477

Como, A., & Mahmoud, H. (2013). Numerical evaluation of tsunami debris impact loading on wooden structural walls. *Engineering Structures*, *56*, 1249–1261. Retrieved from http://dx.doi.org/10.1016/j.engstruct.2013.06.023.

Crespo, A. J. C., Dominguez, J. M., Barreiro, A., Gómez-Gesteira, M., & Rogers, B. D. (2011). GPUs, a new tool of acceleration in CFD: Efficiency and reliability on smoothed particle hydrodynamics methods. *PLoS ONE*, *6*(6).

Crespo, A. J. C., Dominguez, J. M., Gesteira, M. G., Barreiro, A., Rogers, B. D., Longshaw, S., … Vacondio, R. (2013). *User Guide for DualSPHysics code v3.0*.

Crespo, A. J. C., Domínguez, J. M., Rogers, B. D., Gómez-Gesteira, M., Longshaw, S., Canelas, R., … García-Feal, O. (2015). DualSPHysics: Open-source parallel CFD solver based on Smoothed Particle Hydrodynamics (SPH). *Computer Physics Communications*, *187*, 204–216.

Crespo, A. J. C., Gomez-Gesteira, M., & Dalrymple, R. A. (2007). Boundary conditions generated by dynamic particles in SPH methods. *Cmc-Computers Materials & Continua*, *5*, 173–184.

Cunningham, L. S., Rogers, B. D., & Pringgana, G. (2014). Tsunami wave and structure interaction: an investigation with smoothed-particle hydrodynamics. *ICE Journal of Engineering and Computational Mechanics*, *167*(EM3), 126–138.

Dalrymple, R. A., Gómez-Gesteira, M., Rogers, B. D., Panizzo, A., Zou, S., Crespo, A. J. C., … Narayanaswamy, M. (2009). *Smoothed particle hydrodynamics for water waves*. in Advances in numerical simulation of nonlinear water waves, ed. Ma, Q., Singapore: World Scientific Publishing.

Dames and Moore. (1980). *Design and construction standards for residential construction in*

tsunami prone areas in Hawaii. Federal Emergency Management Agency, Washington, D.C.

Farahani, R. J., Dalrymple, R. A., Hérault, A., & Bilotta, G. (2014). Three-dimensional SPH modeling of a bar/rip channel system. *Journal of Waterway, Port, Coastal, and Ocean Engineering*, *140*(1), 82–99.

FEMA. (2003). *Coastal Construction Manual*. (3 vols.) 3rd ed. (FEMA 55). Federal Emergency Management Agency, Jessup, MD.

FEMA (Federal Emergency Management Agency). (2011). *Coastal Construction Manual*. *FEMA P-55* (Vol. II). Washington, DC, USA.

Fujima, K., Achmad, F., Shigihara, Y., & Mizutani, N. (2009). A Study on Estimation of Tsunami Force Acting on Structures. *Journal of Disaster Research*, *4*(6), 404–409.

Gomez-Gesteira, M., Crespo, A. J. C., Rogers, B. D., Dalrymple, R. A., Dominguez, J. M., & Barreiro, A. (2012). SPHysics - development of a free-surface fluid solver - Part 2: Efficiency and test cases. *Computers and Geosciences*, *48*(2), 300–307.

Gomez-Gesteira, M., Rogers, B. D., Crespo, A. J. C., Dalrymple, R. A., Narayanaswamy, M., & Dominguez, J. M. (2012). SPHysics – development of a free-surface fluid solver – Part 1: Theory and formulations. *Computers & Geosciences*, *48*(1), 289–299.

International Code Council. (2009). *2009 International residential code for one- and two-family dwellings*. Country Club Hills, IL.

IOC (Intergovernmental Oceanographic Commission). (2013). *Tsunami Glossary* (Revised Ed). UNESCO, IOC Technical Series, 85, Paris: United Nations Educational, Scientific and Cultural Organization.

Kleefsman, K. M. T., Fekken, G., Veldman, A. E. P., Iwanowski, B., & Buchner, B. (2005). A Volume-of-Fluid based simulation method for wave impact problems. *Journal of Computational Physics*, *206*, 363–393.

Lacroix, D. N., & Doudak, G. (2014). Investigation of Dynamic Increase Factors in Light-Frame Wood Stud Walls Subjected to Out-of-Plane Blast Loading. *Journal of Structural Engineering, ASCE*, 1–10.

Lind, S. J., Xu, R., Stansby, P. K., & Rogers, B. D. (2012). Incompressible smoothed particle hydrodynamics for free-surface flows: A generalised diffusion-based algorithm for stability and validations for impulsive flows and propagating waves. *Journal of Computational Physics*, *231*(4), 1499–1523.

Linton, D., Gupta, R., Cox, D., van de Lindt, J., Oshnack, M. E., & Clauson, M. (2013). Evaluation of Tsunami Loads on Wood Frame Walls at Full Scale. *Journal of Structural Engineering*, *139*(8), 1318–1325.

Longshaw, S. M., & Rogers, B. D. (2015). Automotive fuel cell sloshing under temporally and spatially varying high acceleration using GPU-based Smoothed Particle Hydrodynamics (SPH). *Advances in Engineering Software*, *83*, 31–44.

McCabe, M., Stansby, P. K., Rogers, B. D., & Cunningham, L. S. (2014). Boussinesq modelling of tsunami and storm wave impact. *ICE Journal of Engineering and Computational Mechanics*, *167*(EM3), 106–116.

Mokos, A., Rogers, B. D., Stansby, P. K., & Domínguez, J. M. (2015). Multi-phase SPH modelling of violent hydrodynamics on GPUs. *Computer Physics Communications*, *196*, 304–316.

Monaghan, J. J. (1992). Smoothed particle hydrodynamics. *Ann. Rev. Astron. Astrophys.*, *30*, 543–574.

Nouri, Y., Nistor, I., Palermo, D., & Cornett, A. (2010). Experimental Investigation of Tsunami Impact on Free Standing Structures. *Coastal Engineering Journal*, *52*(01), 43–70.

Okada, T., Sugano, T., Ishikawa, T., Ohgi, T., Takai, S., & Hamabe, C. (2005). *Structural design methods of buildings for tsunami resistance (SMBTR)*. The Building Center of Japan, Japan.

Palermo, D., Nistor, I., Nouri, Y., & Cornett, A. (2009). Tsunami loading of near-shoreline structures: a primer. *Canadian Journal of Civil Engineering*, *36*(11), 1804–1815. http://doi.org/10.1139/L09-104.

Robertson, I. N., Riggs, H. R., Paczkowski, K., & Mohamed, A. (2011). Tsunami bore forces on walls. In *Proceedings of the ASME 2011, 30th International Conference on Ocean, Offshore and Arctic Engineering* (pp. 1–9). Rotterdam, The Netherlands.

St-Germain, P., Nistor, I., Townsend, R., & Shibayama, T. (2014). Smoothed-Particle Hydrodynamics Numerical Modeling of Structures Impacted by Tsunami Bores. *Journal of Waterway, Port, Coastal, and Ocean Engineering*, *140*(1), 66–81.

Suppasri, A., Shuto, N., Imamura, F., Koshimura, S., Mas, E., & Yalciner, A. C. (2013). Lessons Learned from the 2011 Great East Japan Tsunami: Performance of Tsunami Countermeasures, Coastal Buildings, and Tsunami Evacuation in Japan. *Pure and Applied Geophysics*, *170*(6), 993–1018.

Violeau, D., & Rogers, B. D. (2016). Smoothed particle hydrodynamics (SPH) for free-surface flows: past, present and future. *Journal of Hydraulic Research*, *54*(1), 1–26.

Yeh, H., Barbosa, A. R., Ko, H., & Cawley, J. (2014). Tsunami Loadings on Structures. *Coastal Engineering*, 1–13.

Zhang, W. (2009). *An Experimental Study and A Three-Dimensional Numerical Wave Basin Model of Solitary Wave Impact on A Vertical Cylinder*. *School of Civil and Construction Engineering*. Oregon State University.

Notations

A_i	tributary area where pressure probe *i* is situated (m^2)
a	particle *a*
B	the breadth of structure (m)
b	particle *b*
D	represent a certain length of 1 m in the SPH model
D_F	the distance of structure from shoreline (m)
d_p	water particle size or the initial spacing of particle (m)
E	Young's modulus of elasticity (m kg s^{-2})
F_i	force at a certain point in a 3-D model (kg m s^{-2})
g	gravitational acceleration (m s^{-2})
H	solitary wave height (m)
h	characteristic smoothing length (m)
h_0	offshore water depth/still water level (m)
h_b	the height of the bore (m)
h_{im}	maximum inundation depth (m)
L	shortest dimension of box in convergence study (m)
L_p	the layers of pressure probes
m	mass of SPH particle (kg)
P_i	pressure at a certain area in a 3-D model (kg m^{-1} s^{-2})
r_{ab}	distance between two particles (m)
ρ	density, density of SPH particle (kg m^{-3})
v	Poisson's ratio
v_j	the velocity of bore (m s^{-1})
W	weighting function or kernel
$\boldsymbol{\Gamma}$	dissipative term
$\boldsymbol{\Pi}_{ab}$	viscosity term